


 Open access • Posted Content • DOI:10.1101/2021.01.13.426558

Molecular dynamic simulation reveals E484K mutation enhances spike RBD-ACE2 affinity and the combination of E484K, K417N and N501Y mutations (501Y.V2 variant) induces conformational change greater than N501Y mutant alone, potentially resulting in an escape mutant — [Source link](#) 

Gard Nelson, Oleksandr Buzko, Patricia Spilman, Kayvan Niazi ...+2 more authors

Published on: 13 Jan 2021 - [bioRxiv](#) (Cold Spring Harbor Laboratory)

Topics: [Conformational change](#)

Related papers:

- [Deep Mutational Scanning of SARS-CoV-2 Receptor Binding Domain Reveals Constraints on Folding and ACE2 Binding.](#)
- [Tracking Changes in SARS-CoV-2 Spike: Evidence that D614G Increases Infectivity of the COVID-19 Virus.](#)
- [Emergence and rapid spread of a new severe acute respiratory syndrome-related coronavirus 2 \(SARS-CoV-2\) lineage with multiple spike mutations in South Africa](#)
- [SARS-CoV-2 501Y.V2 escapes neutralization by South African COVID-19 donor plasma.](#)
- [Escape from neutralizing antibodies by SARS-CoV-2 spike protein variants.](#)

Share this paper:    

View more about this paper here: <https://typeset.io/papers/molecular-dynamic-simulation-reveals-e484k-mutation-enhances-4vbf2rhn4g>

1 **Molecular dynamic simulation reveals E484K mutation enhances spike RBD-ACE2 affinity and the**
2 **combination of E484K, K417N and N501Y mutations (501Y.V2 variant) induces conformational**
3 **change greater than N501Y mutant alone, potentially resulting in an escape mutant**
4

5 Gard Nelson¹, Oleksandr Buzko¹, Patricia, Spilman¹, Kayvan Niazi¹, Shahrooz Rabizadeh¹,
6 Patrick Soon-Shiong¹

7 ¹ImmunityBio, Inc.

8

9 **Abstract**

10 Rapidly spreading SARS-CoV-2 variants present not only an increased threat to human health
11 due to the confirmed greater transmissibility of several of these new strains but, due to
12 conformational changes induced by the mutations, may render first-wave SARS-CoV-2
13 convalescent sera, vaccine-induced antibodies, or recombinant neutralizing antibodies (nAbs)
14 ineffective. To be able to assess the risk of viral escape from neutralization by first-wave
15 antibodies, we leveraged our capability for Molecular Dynamic (MD) simulation of the spike
16 receptor binding domain (S RBD) and its binding to human angiotensin-converting enzyme 2
17 (hACE2) to predict alterations in molecular interactions resulting from the presence of the E484K,
18 K417N, and N501Y variants found in the South African 501Y.V2 strain – alone and in
19 combination. We report here the combination of E484K, K417N and N501Y results in the highest
20 degree of conformational alterations of S RBD when bound to hACE2, compared to either E484K
21 or N501Y alone. Both E484K and N501Y increase affinity of S RBD for hACE2 and E484K in
22 particular switches the charge on the flexible loop region of RBD which leads to the formation of
23 novel favorable contacts. Enhanced affinity of S RBD for hACE2 very likely underpins the greater
24 transmissibility conferred by the presence of either E484K or N501Y; while the induction of

25 conformational changes may provide an explanation for evidence that the 501Y.V2 variant,
26 distinguished from the B.1.1.7 UK variant by the presence of E484K, is able to escape
27 neutralization by existing first-wave anti-SARS-CoV-2 antibodies and re-infect COVID-19
28 convalescent individuals.

29

30 **Introduction**

31 As many SARS-CoV-2 variants emerge and displace first-wave viruses^{1,2}, it is important not
32 only to assess their relative transmissibility, but also their ability to escape antibody neutralization
33 by convalescent antibodies in recovered COVID-19 patients³, recombinant neutralizing antibodies
34 (nAbs) developed as therapeutics, or antibodies elicited by first-generation vaccines.

35 Of great interest are variants that include mutations with the potential to affect the interaction
36 of the SARS-CoV-2 spike receptor binding domain (S RBD) with the host receptor, angiotensin-
37 converting enzyme 2 (ACE2). The binding of the S RBD of SARS-CoV-2, like SARS-CoV before
38 it, to ACE2 initiates infection⁴⁻⁷, thus variants that have a greater binding affinity for ACE2 are
39 likely to be more readily transmissible⁸. Transmissibility goes hand-in-hand with mortality,
40 because even if a variant does not produce a higher rate of morbidity or mortality, the total number
41 of severe cases and death would be expected to increase due to what may be an exponential
42 increase in infections.

43 The dire consequences of more rapid and widespread infection can further be compounded by
44 a decrease in efficacy of available antibody-based therapeutics and vaccines; and by a loss of
45 protective immunity in persons previously infected with a ‘first wave’ virus. The efficacy of
46 vaccines may be altered if a specific mutation or combination of mutations in a variant results in
47 significant conformational changes that render key regions of S that participate in ACE2 binding

48 ‘unrecognizable’ to antibodies generated in response to a first-generation vaccine. A similar
49 principle is in play for the efficacy of nAbs targeted to the receptor interface^{9,10} and convalescent
50 sera.

51 Here, to better understand the risks posed by individual or combined mutations in the ‘second-
52 wave’ variants, we leveraged our *in silico* Molecular Dynamic (MD) simulation capabilities to
53 perform computational analysis of interactions of the S RBD with human ACE2. In our first report,
54 Nelson *et al.*¹¹ (in preprint) “*Millisecond-scale molecular dynamics simulation of spike RBD*
55 *structure reveals evolutionary adaption of SARS-CoV-2 to stably bind ACE2*”, we initially used
56 millisecond-scale MD simulation to simulate free SARS-CoV-2 S RBD based on previously
57 reported structures^{12,13} as well as its molecular interactions with ACE2 and showed S adopts a
58 binding-ready conformation, incurring little entropic penalty during ACE2 interaction. We further
59 revealed areas of high-affinity interaction between S RBD and ACE2 that have a high likelihood
60 of determining binding kinetics.

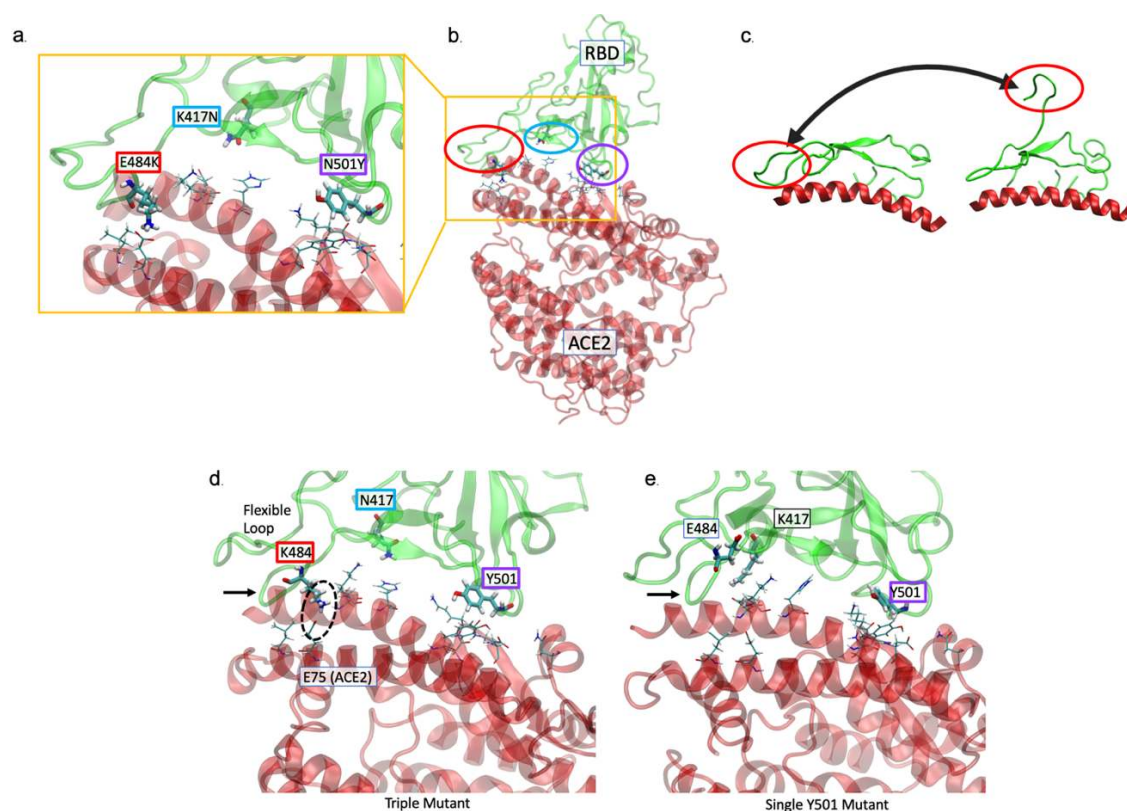
61 Here, we utilized the MD simulation methods employed in our first study to investigate what
62 effects mutations found at the S RBD-ACE2 interface in the rapidly spreading South African
63 variant 501Y.V2¹⁴ - E484K, K417N, and N501Y – have on RBD binding affinity and spike
64 conformation.

65 **Results**

66 As shown in Figure 1a, the E484K, K417N, and N501Y mutants span the S RBD-ACE2
67 interface, with the E484K substitution occurring in a highly flexible loop region of the S RBD
68 (Fig. 1c). The N501Y substitution is found in a second region of contact¹¹, and the K417N mutation
69 in a region between the two that shows relatively little interaction with ACE2.

70 ***E484K shows enhanced affinity for ACE2***

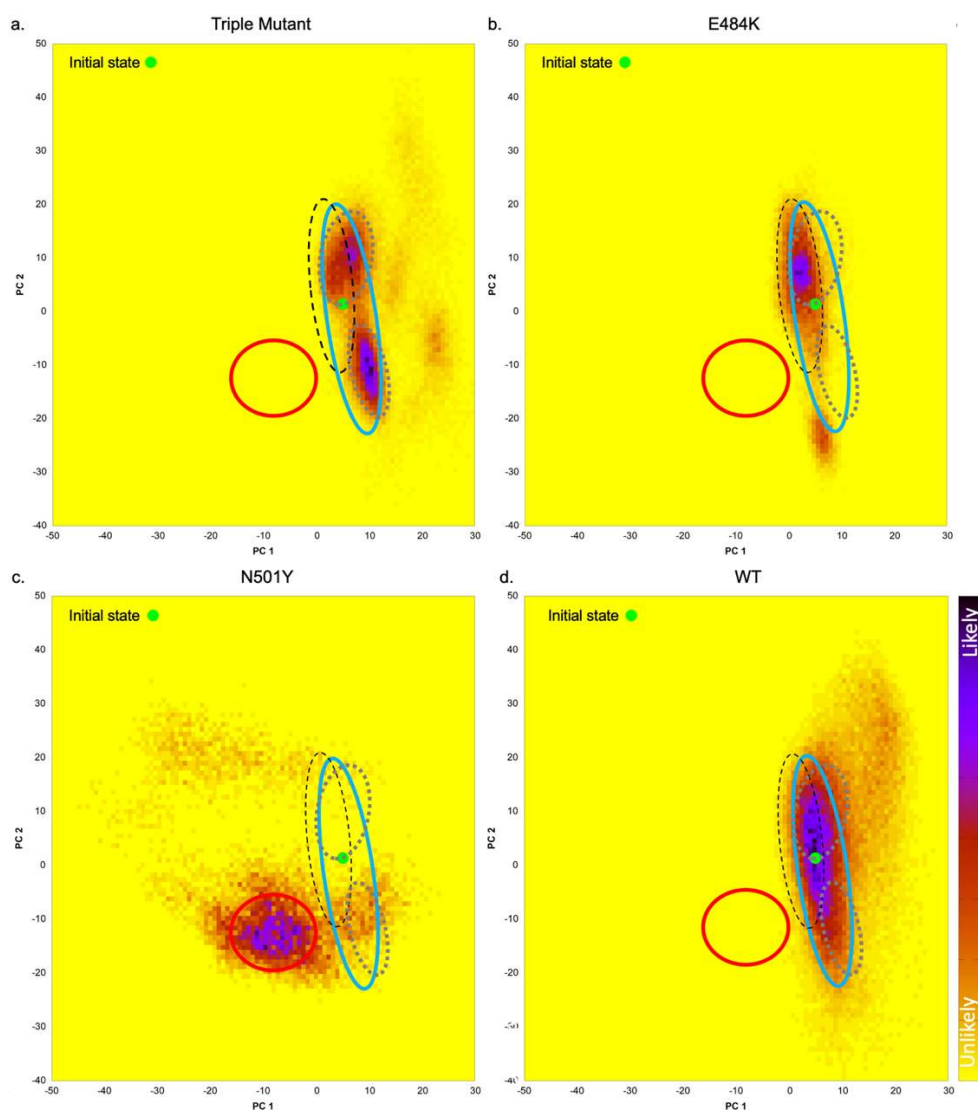
71 As revealed by our MD simulation, the presence of a lysine residue at position 484 in the
72 presence of the other two substitutions (an asparagine residue at position 417; a tyrosine residue
73 at position 501) resulted in increased affinity at position 484 that can be described as the loop being
74 ‘locked onto’ ACE2 (Fig. 1d) as compared to when a glutamic acid residue is present at position
75 484 (Fig. 1e) and a tyrosine at 501. This increased affinity of K484 for hACE2 may be due, in part,
76 to the change in net charge on the flexible loop from -1 to +1. This allows the formation of a
77 transient contact ion pair with E75 in hACE2.



78
79 **Fig. 1** The K484 substitution in the novel South African variant increases affinity of the spike
80 receptor binding domain (S RBD) for ACE2. (a, b) The positions of the E484K (red), K417N
81 (cyan), and N501K (purple) substitutions at the interface of the 501Y.V2 variant S RBD - hACE2
82 interface are shown. hACE2 residues nearest to the mutated RBD residues are rendered as thin
83 sticks. The E484K mutation is located in a highly flexible loop region of the interface, K417N in
84 a region with lower probability of contact, and N501K at a second point of high-affinity contact.
85 (c) The range of movement available to the loop containing residue 484 is shown by PCA of MD
86 simulation of a first-wave sequence^{11,13}. (d) MD simulation performed in the presence of all 3
87 substitutions reveals the loop region is tightly associated (black arrow) with hACE2. A key contact
88 ion pair is circled. (e) In comparison to K484, when E484 (‘wildtype’) is present with only the
89 Y501 variant, the loop is not as tightly associated (arrow).

90 ***E484K in combination with K417N, and N501Y induces conformational changes in spike***

91 To determine if it is likely the presence of the E484K or N501Y mutations alter the
92 conformation of S RBD, we performed Principal Component Analysis (PCA) for the triple mutant,
93 E484K and N501Y mutants alone, and compared them to the original cryo-EM¹³ structure
94 representing the ‘first wave’ sequence. The PCA plots are shown in Figure 2. While both mutants
95 sample similar conformations, S RBD with K484 alone (Fig. 2b) preferentially adopts
96 conformations similar to the cryo-EM structure described in Wrapp *et al.*¹³. This is similar to the
97 behavior observed for the first-wave strain as described in our initial report¹¹. Y501 alone (Fig.
98 2c) affects conformational probability, shifting it away from the original structure. For K484, the
99 effect of the contact ion pair is notable as a distinct density in the black dashed circled region of
100 Figure 2b. When all 3 mutations are present (Fig. 2a), other conformations as indicated by the
101 circled regions, are much more likely to occur compared to the original cryo-EM structure,
102 particularly compared to the Y501 alone (Fig. 2c). With the triple mutant, there is a group of
103 conformations that show good overlap with, and therefore high similarity to, the K484 and WT
104 simulations. There is also a cluster of conformations in a region that is unique to the triple mutant,
105 likely reflecting the influence of the other mutations. Only the WT RBD includes the cryo-EM
106 structure in a region of high probability density (Fig. 2d). The mutated variants adopt novel
107 conformations with varying degrees of distance from the cryo-EM structure. Notably, the single
108 mutants (E484K and N501Y) have a clearly preferred family of conformations while the PCA
109 density of the triple mutant suggests there exists an equilibrium between two distinct states.

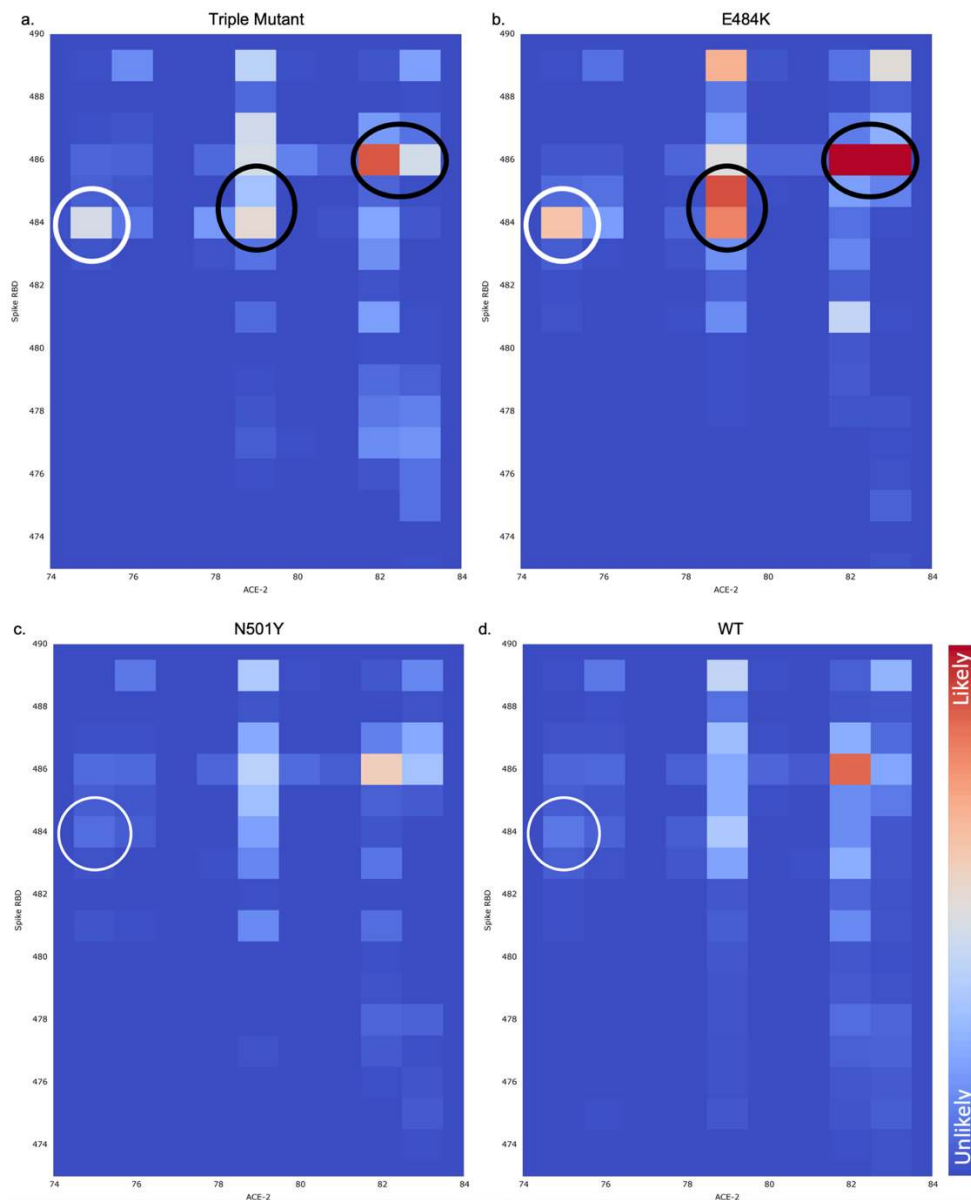


110
111 **Fig. 2** Presence of the E484K mutations alters the conformation of S RBD. Principal component
112 analysis (PCA) plots are shown comparing the accessible conformational space for (a) the triple
113 mutant comprising E484K, K417N, and N501Y; (b) the E484K mutant only; (c) the N501Y mutant
114 only; and (d) the ‘first wave’ sequence to compare the accessible conformational space of each S
115 RBD when bound to hACE2. The green dot indicates the location of the cryo-EM structure, PDB
116 6M17¹³. The blue circled regions indicate conformations that are similar to the original cryo-EM
117 structure, the red circled region to those found for N501Y, the black dashed circle those found for
118 K484 alone, and the gray dashed circles those found for the triple mutant; with a greater density
119 (purple) indicating a greater probability other conformations occur.

120
121 ***E484K shows increased contact with hACE2 E75***

122 E484K, whether in the presence of both K417N, and N501Y variants (Fig. 3a), or as the only
123 variant in the presence of K417 and N501 (Fig. 3b) is associated with increased contact between

124 RBD residue 484 and ACE2 E75 compared to either the N501Y mutant alone or the ‘first wave’
125 (WT) sequence (Fig. 3c and d, respectively). In the presence of either Y501 and WT, E484 shows
126 little contact with hACE2 E75. In addition, The RBD E484K mutant shows increased contact
127 between it and several residue pairs in addition to hACE2 E75.



128 **Fig. 3** Contact maps for position 84 and hACE2 E75. Contact maps are shown for (a) the triple
129 mutant, (b) E484K, (c) N501Y, and (d) ‘wildtype’ spike. Both the triple mutant and the E484K
130 mutant alone show more contact between RBD position 84 and ACE2 E75 (white circles) than
131 N501Y or wildtype (WT or ‘first wave’ sequence). The RBD E484K mutant also shows increased
132 contact with several other residue pairs (black circles). The color scale is consistent across the
133 plots.
134

135 **Discussion**

136 Our MD simulation-based predictions of greater affinity of K484 S RBD for ACE2 as
137 compared to E484 and the greater likelihood of altered conformation as compared to the original
138 structure may represent mechanisms by which the new 501Y.V2 virus variant has been able to
139 replace original viral strains. The enhanced affinity likely accounts for by rapid spread due to
140 greater transmissibility and the likelihood of adoption of conformations not recognized by first-
141 wave antibodies may explain escape of the virus from immunity to the original strain¹⁴.

142 The strong contacts seen for only the E484K mutant here suggest that spike may adopt a
143 distinct ‘binding pose’ relative to other conformations. We further posit the differing PCA
144 densities seen for the triple mutant that seem to result in lesser loop interaction with hACE2 as
145 compared to E484K alone may be due to the other mutations. We will investigate this in depth in
146 future studies.

147 The greater relative risk posed by variants expressing the E484K mutant as compared to the
148 N501Y mutant alone is supported by Andreano *et al.* (in preprint)¹⁵ who co-incubated what they
149 refer to as ‘authentic’ virus with highly neutralizing COVID-19 neutralizing plasma over several
150 passages and saw the appearance of mutations including the E484K substitution which, in
151 combination with an insertion in the spike N-terminal domain (NTD), led to complete resistance
152 to the convalescent plasma. In contrast, Xie *et al.*¹⁶ (in preprint) reported that sera from 20
153 individuals that received the BNT162b2 mRNA vaccine showed equivalent ability to neutralize
154 both Y501 and N501 SARS-CoV-2.

155 Additional support for the threat posed by mutations at residue 484 is provided by Greaney *et*
156 *al.*¹⁷ who undertook an impressive effort to map mutations that affect binding of ten human
157 monoclonal antibodies. By employing a deep mutational scanning method, they found that

158 mutations at residue 484 have a high probability of affecting antibody binding. They further
159 suggested their analytical method provides a tool for design of escape-resistant antibody cocktails
160 to overcome the threat posed by viral evolution. We believe the MD simulation approach used
161 here similarly represents a tool to be used in the arsenal against the continuing pandemic, as it
162 provides insight into the likelihood mutations alone or in combination may have effects that lessen
163 the efficacy of existing therapies or vaccines.

164 In vaccine design, it has been suggest that the makers of vaccines could keep up with viral
165 evolution by continual alteration of the ‘payload’ - almost all vaccines in development use the
166 spike sequence - to fit currently predominant strains. We suggest vaccines whose efficacies are
167 largely dependent upon humoral responses to the S antigen only are inherently limited by the
168 emergence of novel strains and dependent upon frequent re-design. In contrast, a vaccine that
169 elicits a vigorous T-cell response that is far less subject to changes due to accruing mutations
170 provides a better, more efficient approach to protection. The ideal vaccine would also deliver a
171 second, conserved antigen such as the SARS-CoV-2 nucleocapsid protein, that very likely will
172 elicit humoral and cell-mediated immune responses that will remain effective, even in the face of
173 a rapidly changing virus.

174 Although not the subject of the investigation described here, we are developing a dual-antigen
175 human adenovirus serotype 5 (Ad5) platform-based vaccine that delivers both a spike protein with
176 a linker to increase cell surface expression and humoral responses (S-Fusion) and the highly
177 antigenic and conserved nucleocapsid (N) protein with a signal sequence (an Enhanced T-cell
178 Stimulation Domain, ETSD) to direct it to subcellular compartments that enhance MHC I and II
179 responses¹⁸. It is our belief that the vaccine, hAd5 S-Fusion + N-ETSD, due to its ability to elicit
180 cell-mediated in addition to humoral immune responses, as shown in both a rodent model¹⁹ and

181 non-human primates²⁰, offers hope to those regions such as South Africa wherein dangerous
182 variants of SARS-CoV-2 have swept the country.

183

184 **Materials and Methods**

185 *System Setup*

186 The WT-ACE2/RBD complex was built from the cryo-EM structure, PDB 6M17 of full-
187 length human ACE2 in the presence of the neutral amino acid transported B⁰AT1 with the S RBD
188 as shown in Yan *et al.*²¹ using RBD residues 336-518 and ACE2 residues 21-614. The appropriate
189 RBD mutations (K417N, E484K and N501Y for the triple mutant and either E484K or N501Y for
190 the single mutants) were introduced and the complex was created using the Amber ff14SB force
191 field²². A thin solvating shell of water was placed around the complex using the RISM program
192 from AmberTools19²³ to determine optimal locations. Bulk waters (40,655, 40,801 and 39,714
193 waters for the triple mutant, E484K and N501Y, respectively) were added to create a sufficient
194 water box and sodium ions (22, 21 and 23 for the triple mutant, E484K and N501Y, respectively)
195 were added at random locations to neutralize the system.

196

197 *Simulation*

198 10 copies of each RBD mutant were minimized, equilibrated and simulated. Minimization
199 occurred in two phases. During the first, the protein and RISM-placed waters were restrained. The
200 second phase minimized the entire system. Dynamics then began and the temperature was ramped
201 from 0 to 300K while restraining the protein and RISM-placed waters. All dynamics used SHAKE
202 restraints on hydrogen-containing bonds and a 2fs timestep. All restraints were then released and
203 the system was equilibrated in the NPT ensemble for 2ns. Finally, the system equilibrated in the

204 NVT ensemble for 100 ns before data collection began. All simulations were performed with the
205 GPU-enabled version of Amber20²³.

206

207 *Principle Component Analysis (PCA)*

208 The backbones of residues at the RBD/hACE2 interface were used for all PCA calculations.

209 Structures were RMSD aligned to the cryo-EM structure. Eigenvectors for the PCA plots were

210 then calculated using the full set of simulations of the triple mutant, E484K and N501Y systems.

211 Simulation structures were projected onto the eigenvectors for each mutation system separately.

212 All calculations were run with cpptraj and plotted using gnuplot.

213

214

215

216

217

218

219

220

221

222

223

224

225

226

227 References

- 228 1 Davies, N. G. *et al.* Estimated transmissibility and severity of novel SARS-CoV-2 Variant
229 of Concern 202012/01 in England. *medRxiv*, 2020.2012.2024.20248822,
230 doi:10.1101/2020.12.24.20248822 (2020).
- 231 2 Plante, J. A. *et al.* Spike mutation D614G alters SARS-CoV-2 fitness. *Nature*,
232 doi:10.1038/s41586-020-2895-3 (2020).
- 233 3 Weisblum, Y. *et al.* Escape from neutralizing antibodies by SARS-CoV-2 spike protein
234 variants. *Elife* **9**, e61312, doi:10.7554/eLife.61312 (2020).
- 235 4 Simmons, G. *et al.* Characterization of severe acute respiratory syndrome-associated
236 coronavirus (SARS-CoV) spike glycoprotein-mediated viral entry. *Proceedings of the*
237 *National Academy of Sciences of the United States of America* **101**, 4240-4245,
238 doi:10.1073/pnas.0306446101 (2004).
- 239 5 Li, F. Structure, Function, and Evolution of Coronavirus Spike Proteins. *Annu Rev Virol* **3**,
240 237-261, doi:10.1146/annurev-virology-110615-042301 (2016).
- 241 6 Hoffmann, M. *et al.* SARS-CoV-2 Cell Entry Depends on ACE2 and TMPRSS2 and Is
242 Blocked by a Clinically Proven Protease Inhibitor. *Cell* **181**, 271-280.e278,
243 doi:10.1016/j.cell.2020.02.052 (2020).
- 244 7 Benton, D. J. *et al.* Receptor binding and priming of the spike protein of SARS-CoV-2 for
245 membrane fusion. *Nature* **588**, 327-330, doi:10.1038/s41586-020-2772-0 (2020).
- 246 8 Zahradník, J. *et al.* SARS-CoV-2 RBD in vitro evolution follows contagious mutation
247 spread, yet generates an able infection inhibitor. *bioRxiv*, 2021.2001.2006.425392,
248 doi:10.1101/2021.01.06.425392 (2021).
- 249 9 Yu, F. *et al.* Receptor-binding domain-specific human neutralizing monoclonal antibodies
250 against SARS-CoV and SARS-CoV-2. *Signal Transduction and Targeted Therapy* **5**, 212,
251 doi:10.1038/s41392-020-00318-0 (2020).
- 252 10 Pinto, D. *et al.* Cross-neutralization of SARS-CoV-2 by a human monoclonal SARS-CoV
253 antibody. *Nature* **583**, 290-295, doi:10.1038/s41586-020-2349-y (2020).
- 254 11 Nelson, G. *et al.* Millisecond-scale molecular dynamics simulation of spike RBD structure
255 reveals evolutionary adaption of SARS-CoV-2 to stably bind ACE2. *bioRxiv*,
256 2020.2012.2011.422055, doi:10.1101/2020.12.11.422055 (2020).
- 257 12 Walls, A. C. *et al.* Structure, Function, and Antigenicity of the SARS-CoV-2 Spike
258 Glycoprotein. *Cell* **181**, 281-292.e286, doi:10.1016/j.cell.2020.02.058 (2020).
- 259 13 Wrapp, D. *et al.* Cryo-EM structure of the 2019-nCoV spike in the prefusion
260 conformation. *Science* **367**, 1260-1263, doi:10.1126/science.abb2507 (2020).
- 261 14 Tegally, H. *et al.* Emergence and rapid spread of a new severe acute respiratory
262 syndrome-related coronavirus 2 (SARS-CoV-2) lineage with multiple spike mutations in
263 South Africa. *medRxiv*, 2020.2012.2021.20248640, doi:10.1101/2020.12.21.20248640
264 (2020).
- 265 15 Andreano, E. *et al.* SARS-CoV-2 escape &emdash;in vitro&emdash; from a highly
266 neutralizing COVID-19 convalescent plasma. *bioRxiv*, 2020.2012.2028.424451,
267 doi:10.1101/2020.12.28.424451 (2020).
- 268 16 Xie, X. *et al.* Neutralization of N501Y mutant SARS-CoV-2 by BNT162b2 vaccine-elicited
269 sera. *bioRxiv*, 2021.2001.2007.425740, doi:10.1101/2021.01.07.425740 (2021).

- 270 17 Greaney, A. J. *et al.* Complete Mapping of Mutations to the SARS-CoV-2 Spike Receptor-
271 Binding Domain that Escape Antibody Recognition. *Cell Host Microbe*, S1931-
272 3128(1920)30624-30627, doi:10.1016/j.chom.2020.11.007 (2020).
- 273 18 Sieling, P. *et al.* Th1 Dominant Nucleocapsid and Spike Antigen-Specific CD4+ and CD8+
274 Memory T Cell Recall Induced by hAd5 S-Fusion + N-ETSD Infection of Autologous
275 Dendritic Cells from Patients Previously Infected with SARS-CoV-2. *medRxiv*
276 <https://doi.org/10.1101/2020.11.04.20225417>, doi:10.1101/2020.11.04.20225417
277 (2020).
- 278 19 Rice, A. *et al.* A Next Generation Bivalent Human Ad5 COVID-19 Vaccine Delivering Both
279 Spike and Nucleocapsid Antigens Elicits Th1 Dominant CD4+, CD8+ T-cell and
280 Neutralizing Antibody Responses. *bioRxiv* <https://doi.org/10.1101/2020.07.29.227595>,
281 doi:10.1101/2020.07.29.227595 (2020).
- 282 20 Gabitzsch, E. *et al.* Complete Protection of Nasal and Lung Airways Against SARS-CoV-2
283 Challenge by Antibody Plus Th1 Dominant N- and S-Specific T-Cell Responses to
284 Subcutaneous Prime and Thermally-Stable Oral Boost Bivalent hAd5 Vaccination in an
285 NHP Study. *bioRxiv*, 2020.2012.2008.416297, doi:10.1101/2020.12.08.416297 (2020).
- 286 21 Yan, R. *et al.* Structural basis for the recognition of SARS-CoV-2 by full-length human
287 ACE2. *Science* **367**, 1444-1448, doi:10.1126/science.abb2762 (2020).
- 288 22 Maier, J. A. *et al.* ff14SB: Improving the Accuracy of Protein Side Chain and Backbone
289 Parameters from ff99SB. *J Chem Theory Comput* **11**, 3696-3713,
290 doi:10.1021/acs.jctc.5b00255 (2015).
- 291 23 Case D.A. *et al.* AMBER 2019. *University of California, San Francisco* (2019).
292
- 293
- 294
- 295
- 296